Hindawi
Geofluids
Volume 2021, Article ID 3615333, 20 pages
https://doi.org/10.1155/2021/3615333

Research Article

X-Ray CT Investigation on Fractal Characteristics of Fine-Grained Tailing Sand in Fujian's Makeng: Insight into the Mesoscopic Seepage Failure

Dayu Long[1,2] **Changhong Li**[1,2] **Yu Wang**[1,2] **and Yueqi Shi**[1,2]

[1]*Key Laboratory of Ministry of Education for High-Efficient Mining and Safety of Metal Mines, University of Science and Technology Beijing, Beijing 100083, China*
[2]*School of Civil and Resource Engineering, University of Science and Technology Beijing, Beijing 100083, China*

Correspondence should be addressed to Yu Wang; wyzhou@ustb.edu.cn

Received 12 October 2021; Accepted 16 November 2021; Published 21 December 2021

Academic Editor: Dongdong Ma

This work is aimed at revealing the mesophysical process and mechanical behaviors of fine-grained tailing sand during seepage failure. The macroscopic seepage tests combined with posttest X-ray computed tomography (CT) were employed to study the fractal characteristics of mesostructure. Results show that before and after the seepage failure of fine-grained tailing sand, fractal of pore distribution (D_{pd}) and fractal dimension of pore size (D_{ps}) show a relatively obvious positive correlation with porosity. Tailing particles migrate along the seepage direction during the seepage process, resulting in the gradual decrease of D_{pd} and pore distribution area. The D_{ps} reflects the variation characteristics of pore number distribution with different pore sizes. The increase in D_{ps} leads to a decrease in the uniformity of pore size and an increase in the size difference between pores. The mass fractal dimension (D_m) of fine-grained tailing sand samples ranges from 1.6472 to 1.8256. With the increase of D_m, the coefficient of uniformity (C_u) of tailing sand tends to increase. The D_m method can discern the seepage failure type of fine-grained tailing sand, and it is more accurate than the traditional method. This study provides a reference for the prevention and control of the seepage failure of tailing dam.

1. Introduction

Tailing sand is the raw material for the tailing dam. It is a special geotechnical medium produced after ore crushing and separation. It is quite different from natural soil in structural characteristics and physicochemical properties [1–3]. Fine tailing sand particles migrate under the action of pore water seepage, which affects the skeleton structure of tailing particles and weakens the structural strength of the tailing dam [4]. It may cause seepage damage and even instability of tailing dam. At present, there have been a lot of studies on the macroscopic seepage characteristics and mechanical behavior of tailing sand, as well as some studies on the mesostructure characteristics [5–10]. Yin et al. [1] studied the effect of seepage on the microstructure of tailing sand and found that the loose particles migrate taken by seepage water, the upper pores become bigger, and lower pores become smaller. By scanning electron microscopy and X-ray CT, Yang et al. [11] found that the silty tailing sand contained granular particles and flake particles, and the surface of sand tailings was rougher. Shi et al. [12] studied the changed characteristics of particle distribution and pore structure of three kinds of fine-grained tailing sand after seepage failure by micro-CT. However, the mesostructure changes of tailing sand seepage failure are extremely complex. The introduction of fractal theory is helpful to study the variation characteristics of mesostructure.

Fractal theory was proposed by Mandelbrot [13]. It provides new ideas for studying the microstructure characteristics of soils and rocks and provides an effective theoretical method for quantitatively characterizing their complex characteristics. Fractal dimension of particle size analyzes the

complex distribution characteristics of particle size and particle number, volume, and mass, which proposes a fractal model of particle number-particle size [14]. Tyler and Wheatcraft [15] established the relationship expression between particle mass fraction and particle size based on the fractal model of particle number-particle size, making the D_m become an important parameter for the grading characteristics of soil particles. The D_m is widely used in the study of the spatial variability of soil particle size distribution, the moisture characteristic curve, and the study of particle breakage under different loading conditions such as uniaxial compression, triaxial compression, and impact load [16–20]. The pore fractal method establishes a fractal model of the mesostructure of soil based on the characteristics of pore distribution or pore size distribution [21, 22]. It provides a theoretical method for quantitatively studying the microstructure characteristics, hydrodynamic characteristics, structural strength, and electrical conductivity of soil [23–29]. Fractal theory is a useful tool for studying the mesostructure of soil and rock. It is rarely used in the study of tailing sand. Jiang [30] studied the fractal characteristics of tailing sand lenses and their influence on the stability of the tailing dam. Zhang et al. [31] quantitatively studied the microscopic characteristics and deformation characteristics of tailing sand based on fractal geometry. However, the available research is rarely involved in analyzing the fractal characteristics of the mesostructure of tailing sand seepage failure.

In this paper, a specially designed seepage failure instrument was used to conduct a macroscopic seepage failure experiment of fine-grained tailing sand, and a CT scanning was performed on the samples after seepage failure. Based on the fractal theory, the fractal characteristics of the mesostructure of tailing seepage failure are studied, and the D_m method is proposed to distinguish the types of tailing sand seepage failure. The research results provide a reliable reference for the treatment of seepage failure of tailing dam.

2. Fractal Theory

2.1. Fractal Dimension of Pore Distribution. In the calculation of the D_{pd} of tailing sand, the D_{pd} of porous media constructed by Sierpinski gasket can be used to describe the distribution of pores [32]. Assuming that the two-dimensional image of area $L \times (\beta L)$ contains multiple particles (β is the ratio of the side length of the x axis to the y axis). The image is divided into an orthogonal grid with a specification of $L/a \times ((\beta L)/a)$ by a square grid with a side length of a. The total number of grids containing pores (or part) is $N(a)$, and it changed a to make it change within a certain range, such as $a_1, a_2, \cdots, a_n$. Then, the sequence values of the corresponding total number of grids, $N(a_1)N(a_1), N(a_2)N(a_2), \cdots, N(a_n)$, are obtained. When determining the length of a, β should be fully considered to ensure that the lengths of both sides can be divisible by a. These data pairs are expressed in the double logarithmic coordinate system, and the $\ln a - \ln N(a)$ correspondence relationship can be determined intuitively. If there are linear features, it indicates that the particle distribution has fractal features:

$$D_{\mathrm{pd}} = \lim_{a \longrightarrow 0} \frac{\log N(a)}{\log 1/a}, \tag{1}$$

where D_{pd} is the fractal dimension of pore distribution.

2.2. Fractal Dimension of Pore Size. Pore size is one of the important parameters of porous media. For a certain porous media, the total number of pores is assumed to be a constant. Generally, the variation of pore number is characterized by the distribution characteristics of the cumulative number $N(\geq r)$ of pores larger than r (r is pore size). According to the distribution characteristics of porous media, $r - N(\geq r)$ has a good power function correspondence [14], namely,

$$N(\geq r) = \int_r^{r_{\max}} p(r) d \propto r^{-D_{\mathrm{ps}}}, \tag{2}$$

where $p(r)$ is the pore size distribution density function; N is the total number of pores, a constant; $r_{\max}$ is maximum pore radius in porous media; $N(r)$ is the number of total pores greater than r.

This is completely consistent in form with the definition of the capacity dimension in fractal geometry (also known as the Kolmogorov capacity dimension), so it can be said that the microscopic pore distribution of porous media has fractal characteristics. In the specific calculation, the pore radius r was taken as the abscissa, and $N(r)$ was taken as the ordinate. The relationship of r and $N(r)$ was determined in the bilogarithmic coordinate system, and the negative slope of the stable straight line part was taken as D_{ps}.

2.3. Fractal Dimension of Particle Size and Mass Fractal Dimension. The particle size distribution of tailing sand has statistical self-similarity. Traditional tailing sand particle size characterization methods cannot further distinguish the subtle differences between tailing sand with different properties. The introduction of the fractal dimension has effectively solved this problem [33]. As one of the basic physical properties of tailing sand, particle size distribution is not only an important content in the study of tailing sand structure but also an important indicator of the seepage failure of tailing sand. For example, fractal dimension of particle size of tailing sand can further compare the particle distribution feature and texture uniformity of different tailing sand [34, 35]. Particle composition is an important parameter of soil. In the two-dimensional plane, it is assumed that the area occupied by particles larger than a certain particle size R is A [15].

$$A(r > R) = C_a \left[1 - \left(\frac{R}{\lambda_a}\right)^{2-D}\right], \tag{3}$$

where r is the measuring scale and C_a and λ_a are parameters related to the size and shape of the particles.

Extend formula (3) from two-dimensional to three-dimensional state; then, the volume of soil larger than a certain particle size R_i is as follows:

$$V(r > R_i) = C_v \left[1 - \left(\frac{R_i}{\lambda_v}\right)^{3-D}\right]. \quad (4)$$

The particles between the two sieves are expressed by their average value $\bar{R}_i$; then, formula (4) can be expressed as follows:

$$V\left(r > \bar{R}_i\right) = C_v \left[1 - \left(\frac{\bar{R}_i}{\lambda_v}\right)^{3-D}\right]. \quad (5)$$

Assuming that the specific gravity of particles at all levels is equal, the mass greater than a certain average particle size $\bar{R}_i$ is as follows:

$$M\left(r > \bar{R}_i\right) = \rho V\left(r > \bar{R}_i\right) = \rho C_v \left[1 - \left(\frac{\bar{R}_i}{\lambda_v}\right)^{3-D}\right]. \quad (6)$$

Assuming that the average particle size is zero, formula (6) represents the mass M_T of all soils, putting M_T into the calculation to obtain the following:

$$\frac{M\left(r > \bar{R}_i\right)}{M_T} = 1 - \left(\frac{\bar{R}_i}{\lambda_v}\right)^{3-D}. \quad (7)$$

Assume that $R_{\max}$ is the maximum particle size of soil; then,

$$\frac{M\left(r < \bar{R}_i\right)}{M_T} = \left(\frac{\bar{R}_i}{R_{\max}}\right)^{3-D_m}, \quad (8)$$

where D_m is the mass fractal dimension of soil particles. The D_m calculation method is as follows: M_R is the cumulative mass of particles smaller than a certain particle size R, and M is the total mass of soil particles. Then, M_R/M and R can be expressed in the double logarithmic coordinates, using the least square method for linear regression fitting, and the slope of the straight line is set to K; then, the D_m of the corresponding soil particles is as follows:

$$D_m = 3 - K. \quad (9)$$

Assuming that the specific gravities of the particles at all levels are equal, the volume ratio V_R/V and R of particles smaller than a certain particle size R can be expressed in the double logarithmic coordinates, and the least square method is used for linear regression fitting. The slope of the straight line is K'; then, the D_m of the corresponding soil particles is as follows:

$$D_{\mathrm{m}} = 3 - K'. \quad (10)$$

3. Experimental Materials and Methods

3.1. Tailing Sand. The tailing sand used in the experiment came from the Makeng tailing pond in Longyan City, Fujian Province, China. The tailing sand was analyzed by X-ray fluorescence spectroscopy (XRF), and it was found that the tailing sand is mainly composed of SiO_2, CaO, Fe_2O_3, MgO, Al_2O_3, and other components. The specific content is shown in Table 1.

Table 1: Chemical composition and content of tailing sand.

Chemical composition	SiO_2	CaO	Fe_2O_3	MgO	Al_2O_3	MnO	Others
Content/%	37.07	26.06	18.47	9.00	3.60	2.07	3.73

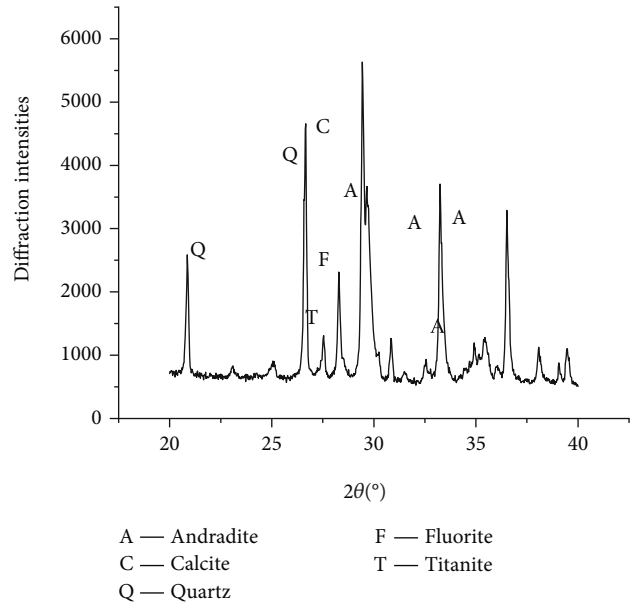

Figure 1: XRD spectrum of tailing sand.

From the results of X-ray diffraction (XRD) analysis of tailing sand, the main mineral components of tailing sand are Calcite, Andradite, Quartz, Fluorite, and Titanite. The specific content is shown in Figure 1.

The five groups of tailing sand were experimented with a laser particle size analyzer to obtain the particle size distribution curve and particle size gradation cumulative curve. The result is shown in Figure 2.

It can be seen from Figure 2 that the composition of the tailing sand particles in the first and second groups is similar, and the content of fine particles smaller than 75 μm is about 25%. However, the distribution curve of the particles in the first group is slower than that in the second group, and the content of fine particles with a diameter of 0-20 μm is accumulated faster in the initial stage.

The content of fine particles with a particle size of less than 75 μm in the third group to the fifth group is, respectively, about 40%, 70%, and 30%. Gradation constants of different groups of tailing sand are shown in Table 2. Five groups of tailing sand are all in a poorly graded state, which has a negative impact on the safety and stability of the tailing dam.

According to the grain size grading accumulative curve, use formula (8) for analysis and calculation to obtain the

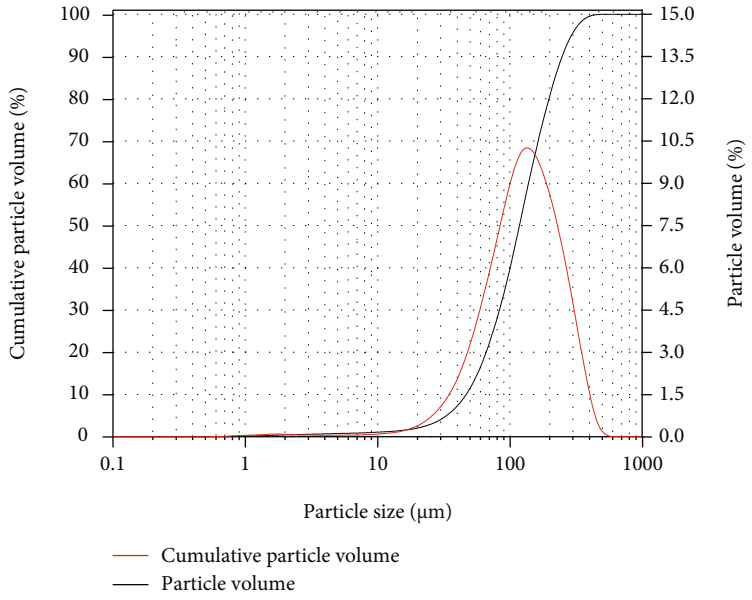

(a)

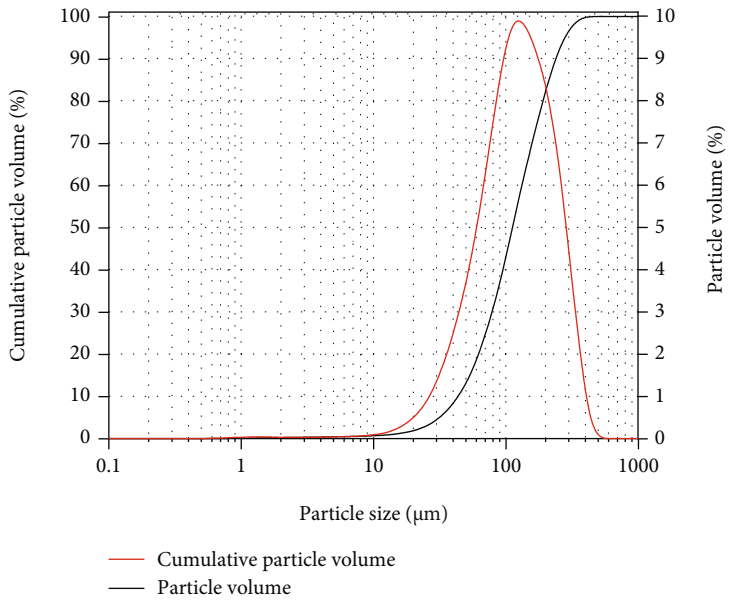

(b)

Figure 2: Continued.

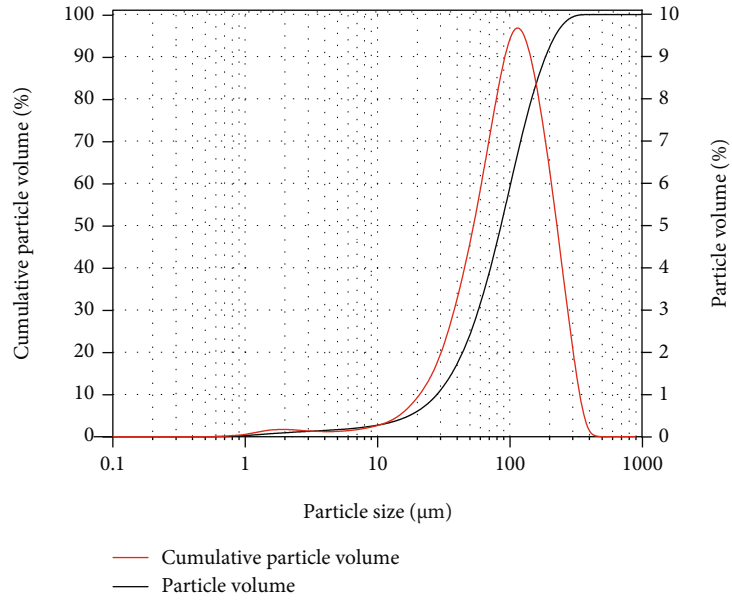

(c)

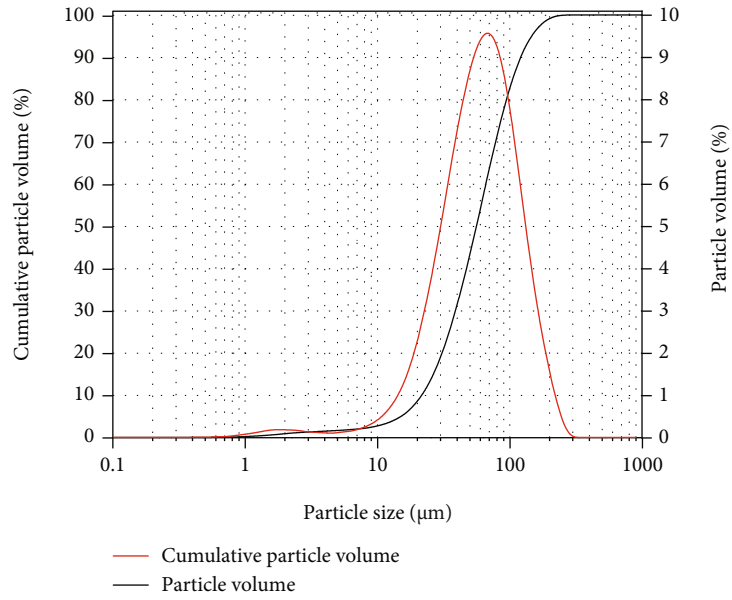

(d)

Figure 2: Continued.

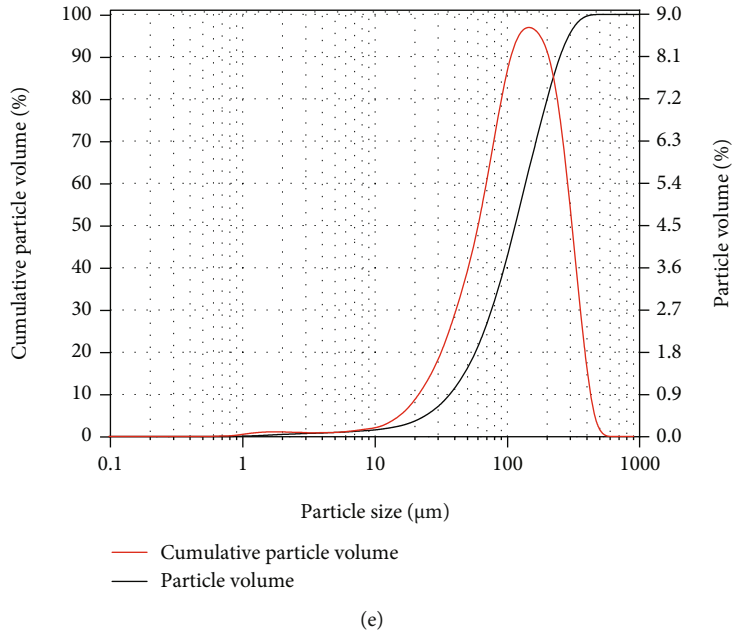

Figure 2: Grain size grading accumulative curve of fine-grained tailing sand: (a) the first group; (b) the second group; (c) the third group; (d) the fourth group; (e) the fifth group.

Table 2: Grading constants of tailing sand of different groups.

Groups	d_{10} (μm)	d_{30} (μm)	d_{50} (μm)	d_{60} (μm)	C_u	C_c
First	47.12	83.88	118.15	147.96	3.14	1.01
Second	47.16	64.22	119.75	137.96	2.92	0.63
Third	30.49	63.32	91.7	106.85	3.50	1.23
Fourth	20.15	37.75	53.37	61.58	3.06	1.15
Fifth	39.78	78.87	112.96	136.03	3.42	1.15

d_{10}: the mass of soil particles smaller than this size is 10% of the total mass of tailing sand particles, which is the effective particle size. d_{30}: the mass of soil particles smaller than this size is 30% of the total mass of tailing sand particles, which is the median particle size. d_{50}: the mass of soil particles smaller than this size is 50% of the total mass of tailing sand particles, which is the average particle size. d_{60}: the mass of soil particles smaller than this size is 60% of the total mass of tailing sand particles, which is the constrained grain size. C_u is the soil coefficient of uniformity obtained from the grain size distribution curve. C_c is the soil curvature coefficient obtained from the grain size distribution curve.

D_m of tailing sand. The results of one to five groups are, respectively, 1.7498, 1.6472, 1.8256, 1.7007, and 1.7805.

3.2. Experimental Equipment. The experiment uses a specially designed seepage failure instrument suitable for fine-grained tailing sand. It is composed of four parts: a lifting water supply device, a pressurized water tank, a sample container, and a piezometer tube, as shown in Figure 3(a). The sample container is a transparent cylinder with an inner diameter of 150 mm and a height of 270 mm, which is convenient for observing experimental phenomena. In the sample container sidewall from bottom to top every 40 mm, set pressure tube joints, a total of five joints. The following four joints are connected with the pressure tube, the top joint as a water outlet to collect seepage flow. After the seepage failure experiment, the tailing sand sample was scanned using a nano Voxel-3000 micro-CT, as shown in Figure 3(b). The highest spatial resolution capability of this instrument is 0.5 μm, which can nondestructively perform three-dimensional visual characterization of the internal microstructure of tailing sand.

3.3. Experimental Procedure. The experiment adopts the method of increasing the head difference step by step to simulate the whole process of the seepage failure of tailing sand. After the seepage failure experiment, layered samples are taken for CT scanning. The specific experimental process is as follows:

(1) *Preparation Stage.* It is according to the selected dry density $\rho = 2.0\,\text{g·cm}^{-3}$ to determine the quality of the tailing sand. Before filling the tailing sand, the vaseline was evenly spread on the tube wall inside the sample container. A 150 mm diameter permeable stone is placed at the bottom of the sample container to ensure uniform and stable water flow during infiltration. Connect the sample container, the pressurized water tank, and the water supply device and then exhaust the air in the pressurized water tank through the exhausting valve, so that the pressurized water tank is filled with water.

(2) *Filling Stage.* Tailing sand is divided into five layers in the sample container and compacted with a tamper after filling. Each layer of tailing sand is rammed to a thickness of 40 mm according to the preset dry density, while ensuring that the sample is as uniform and smooth as possible. After each layer of tailing sand is filled, open the water supply valve until the

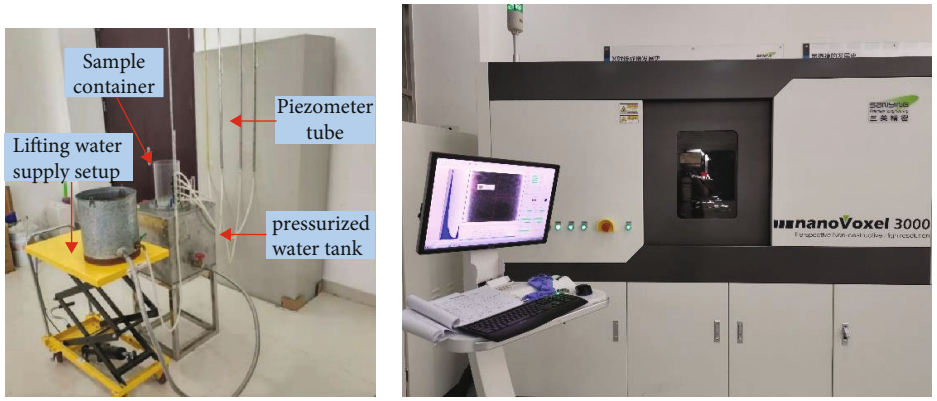

(a) (b)

Figure 3: Experimental equipment: (a) a specially designed seepage failure instrument; (b) a nano Voxel-3000 micro-CT system.

surface of the tailing sand begins to bleed. Then, connect the pressure tube and remove the bubbles in the tube. Before adding the next layer of tailing sand, a silica gel sealing ring is placed on the surface of it to prevent concentrated seepage along the sidewall from affecting the experimental results. After tailing sand filling, raise the water head height of the water supply device until the outlet of the sample container gives water. At this time, the initial water head height of the experiment is reached, and the water head is kept stable. After standing for 24 hours, it is considered that the tailing sand has reached saturation.

(3) *Experimental Stage*. After the tailings are saturated, seepage begins to occur, and the seepage flow for 5 minutes is collected by a measuring cylinder, and the data is recorded. When the seepage flow is stable and the value of the piezometer is constant, the reading of the piezometer is recorded. The height of the water head is increased step by step by adjusting the height of the lifting water supply device, and it increases by 2 cm each time. The readings are recorded after 10 minutes of stabilization until the tailing sand sample is damaged by the seepage force. Pay attention to observing experimental phenomena during the experiment. When there are obvious cracks or slight uplift on the surface of the tailing sand sample, or cracks and faults appear on the tailing sand, it indicates that the sample has reached the critical failure. At this time, the readings of each piezometer tube are recorded to calculate the hydraulic gradient, which is the critical hydraulic gradient (i_{cr}) of the seepage failure of the sample. With the gradual increase of the water head, when the seepage flow suddenly increases, it is considered that the sample has been destroyed at this time, and the experiment is stopped. The sample of tailing sand during the seepage failure process is shown in Figure 4

The first group of tailing sand sample is sampled layer by layer for CT scanning after seepage failure to obtain the microstructure characteristics of the pores. After the seepage

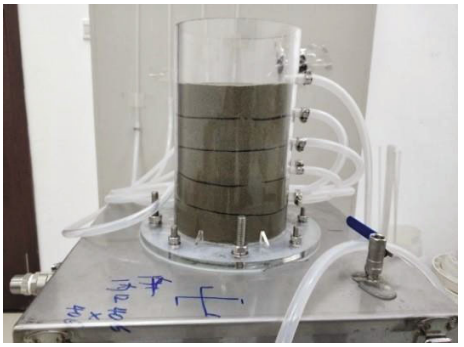

Figure 4: Tailing sand sample during the seepage failure.

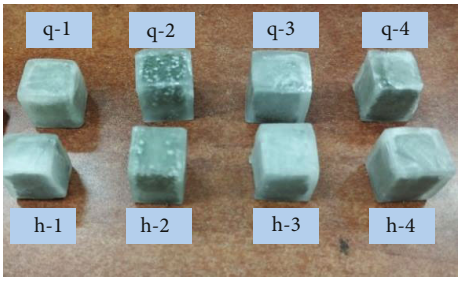

Figure 5: Wax-seal tailing sand sample.

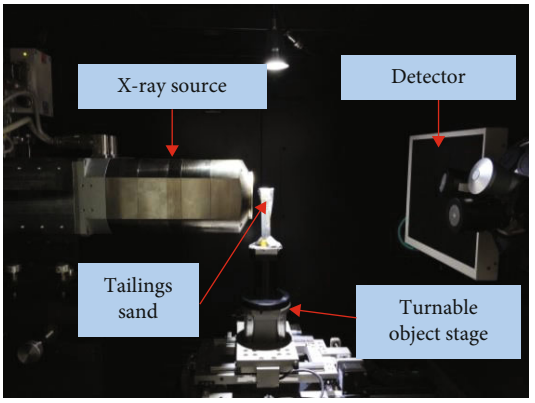

Figure 6: Micro-CT scanning of tailing sand.

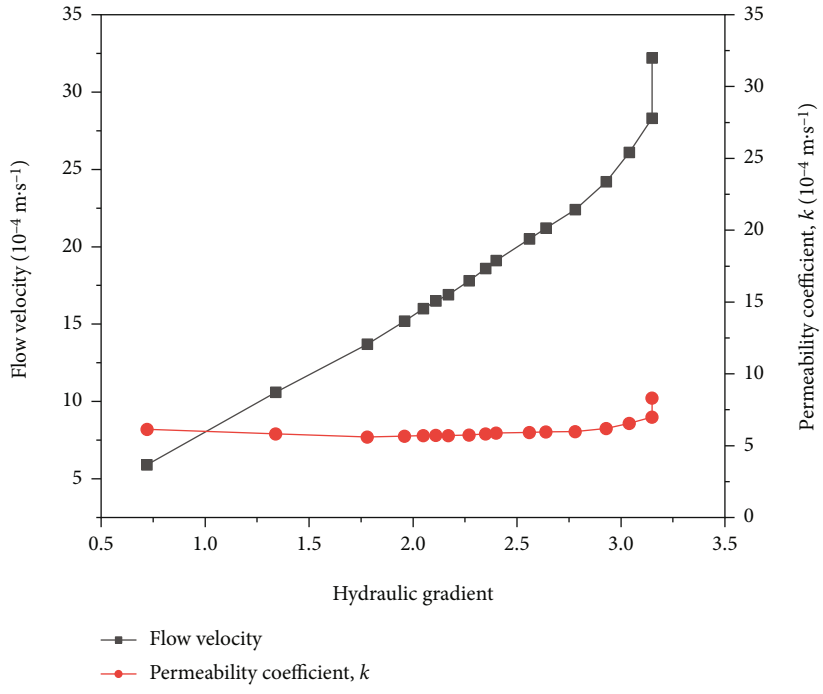

(a)

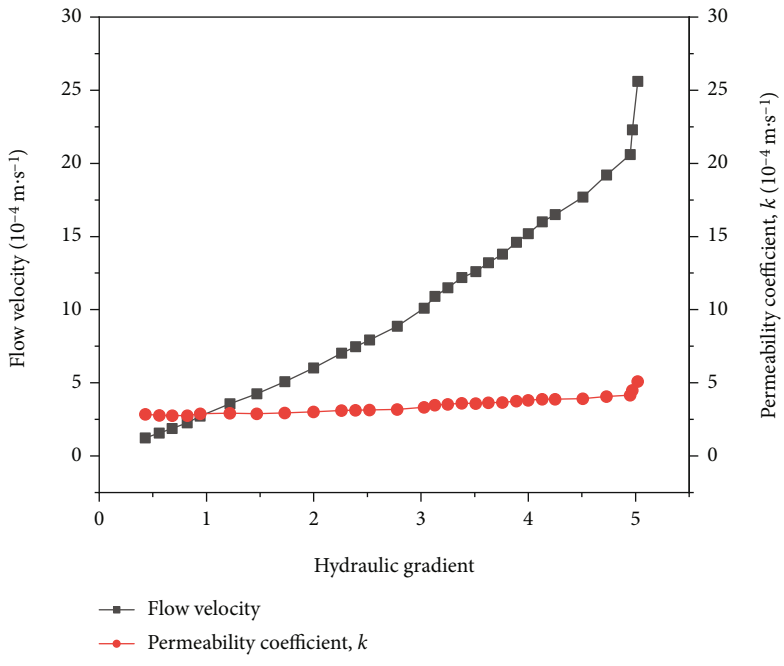

(b)

Figure 7: Continued.

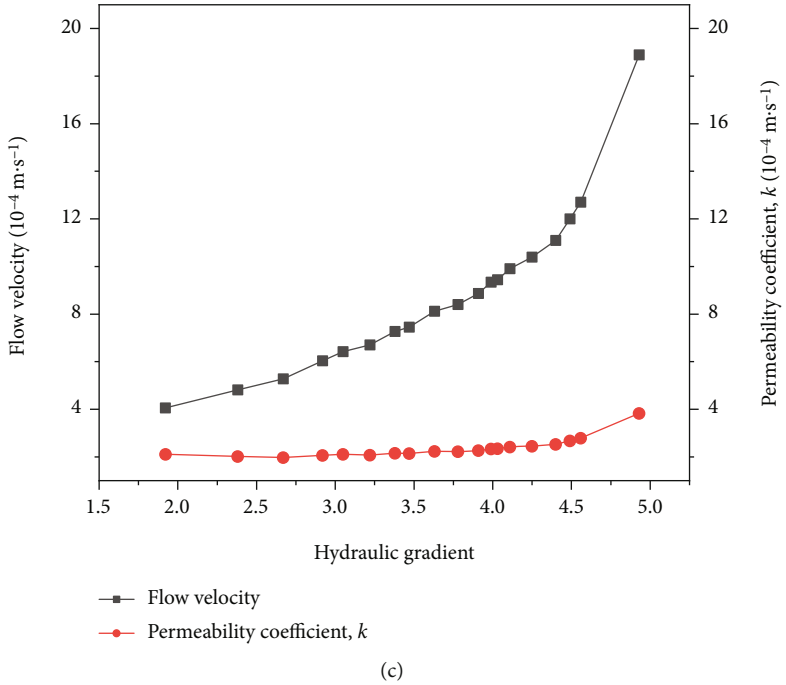

(c)

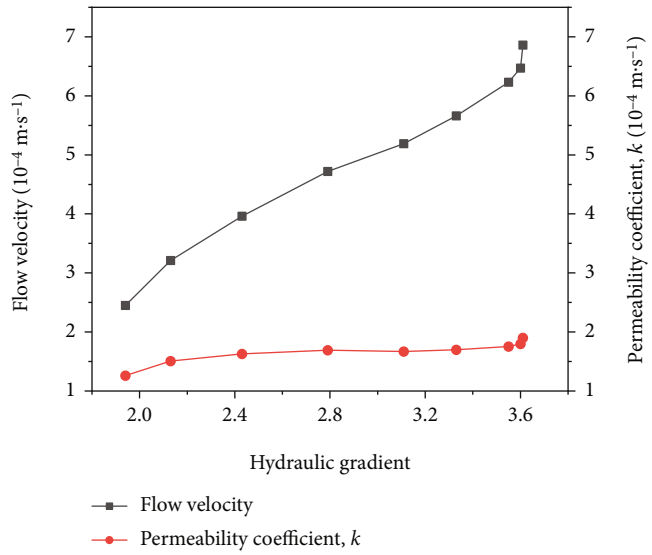

(d)

Figure 7: Continued.

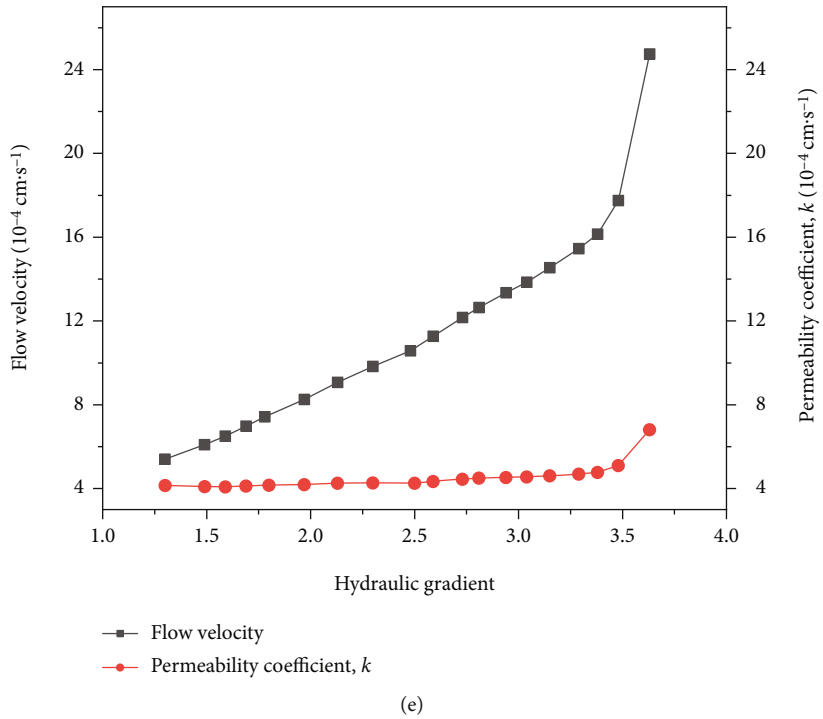

(e)

Figure 7: The relationship curve of the hydraulic gradient with seepage velocity and permeability coefficient: (a) the first group; (b) the second group; (c) the third group; (d) the fourth group; (e) the fifth group.

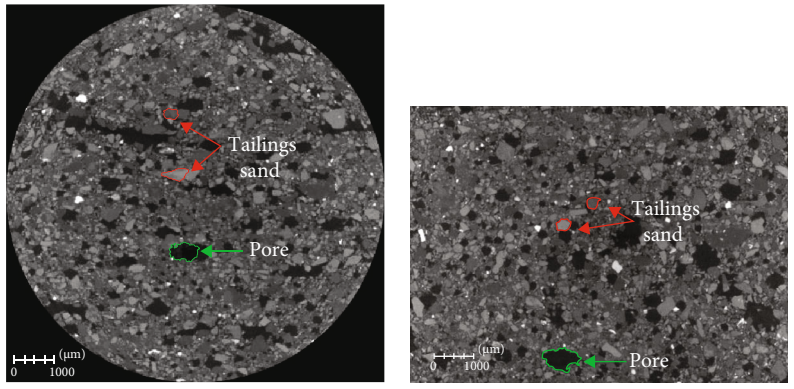

(a) (b)

Figure 8: Two-dimensional section diagram of tailing sand sample: (a) x-y direction; (b) x-z direction.

failure of the first group of tailings, stratified sampling from bottom to top is carried out for CT scanning. The sampling positions are 0-40 mm for the first layer, 40 mm-80 mm for the second layer, 80 mm-120 mm for the third layer, and 120 mm-160 mm for the fourth layer. All samples are cube with a side length about 15 mm, numbered h-1, h-2, h-3, and h-4, and sealed with paraffin after sampling to facilitate CT scanning. At the same time, set up a control group. The first group of tailing sand is filled into the specially designed seepage failure instrument, and the saturated sample is used as the sample before the seepage failure. Scan samples are taken in layers at the same sampling position, numbered q-1, q-2, q-3, and q-4, with a total of eight CT scan samples, as shown in Figure 5. CT scanning of tailing sand is shown in Figure 6.

By adjusting the micro-CT scan parameters, making the tailing sand sample gets the best imaging effect. In the experiment, the voltage, the current, exposure time, and resolution were, respectively, 140 kV, 70 μA, 0.80 s, and 7.57 μm. A cone beam continuous scanning method was adopted in the experiment, and the scanning rate was 0.25°/frame, with 1440 projections in total.

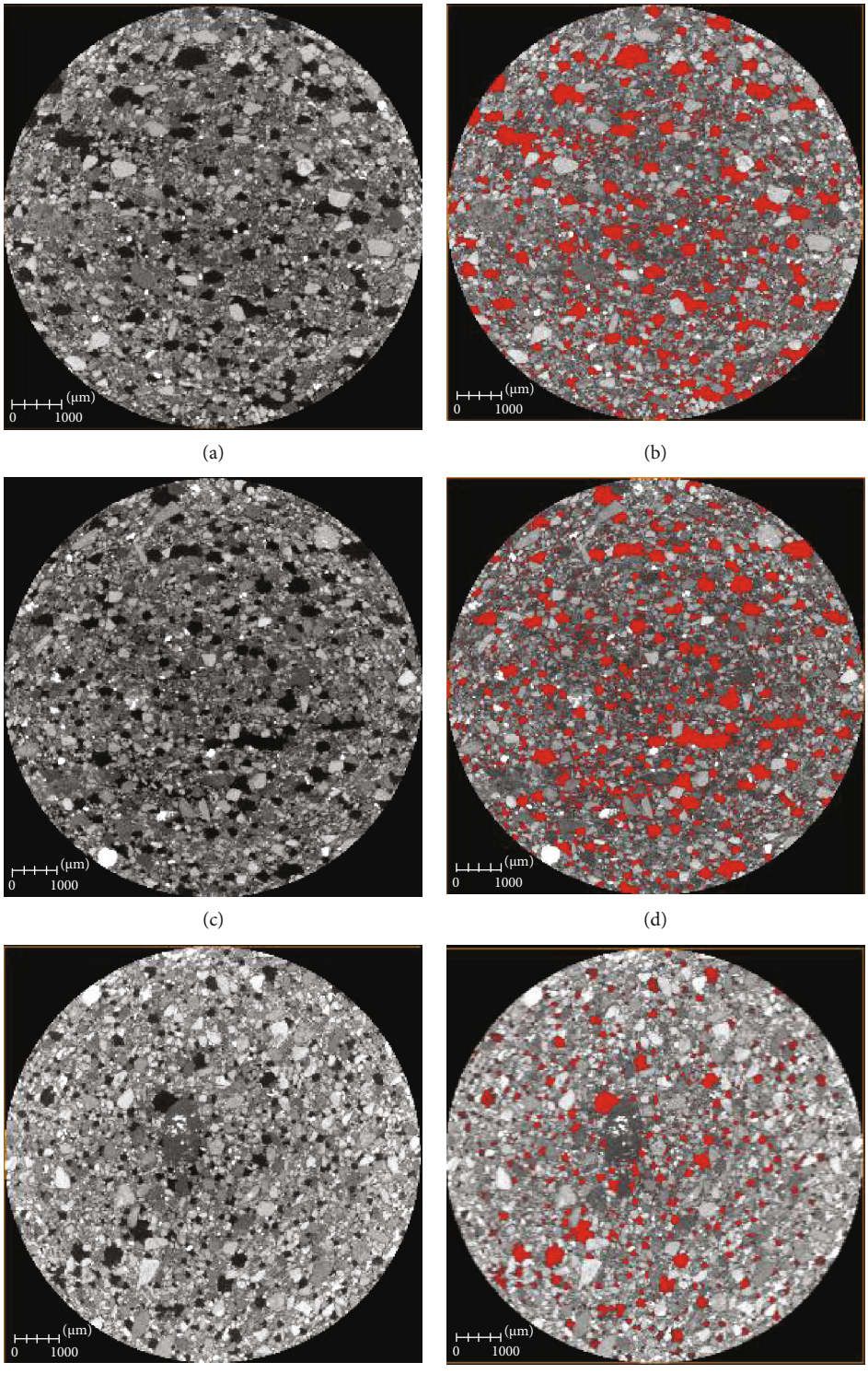

Figure 9: Continued.

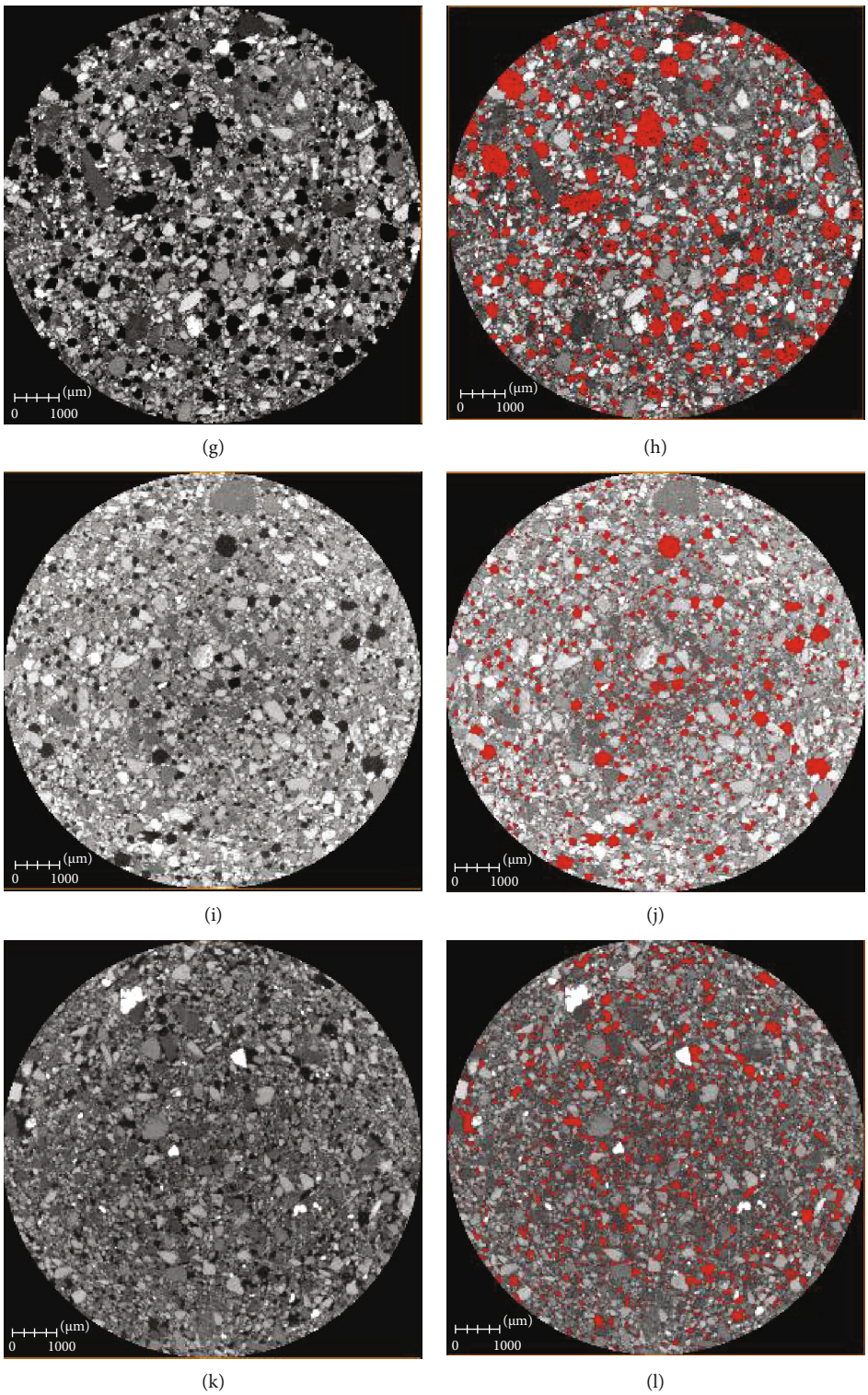

Figure 9: Continued.

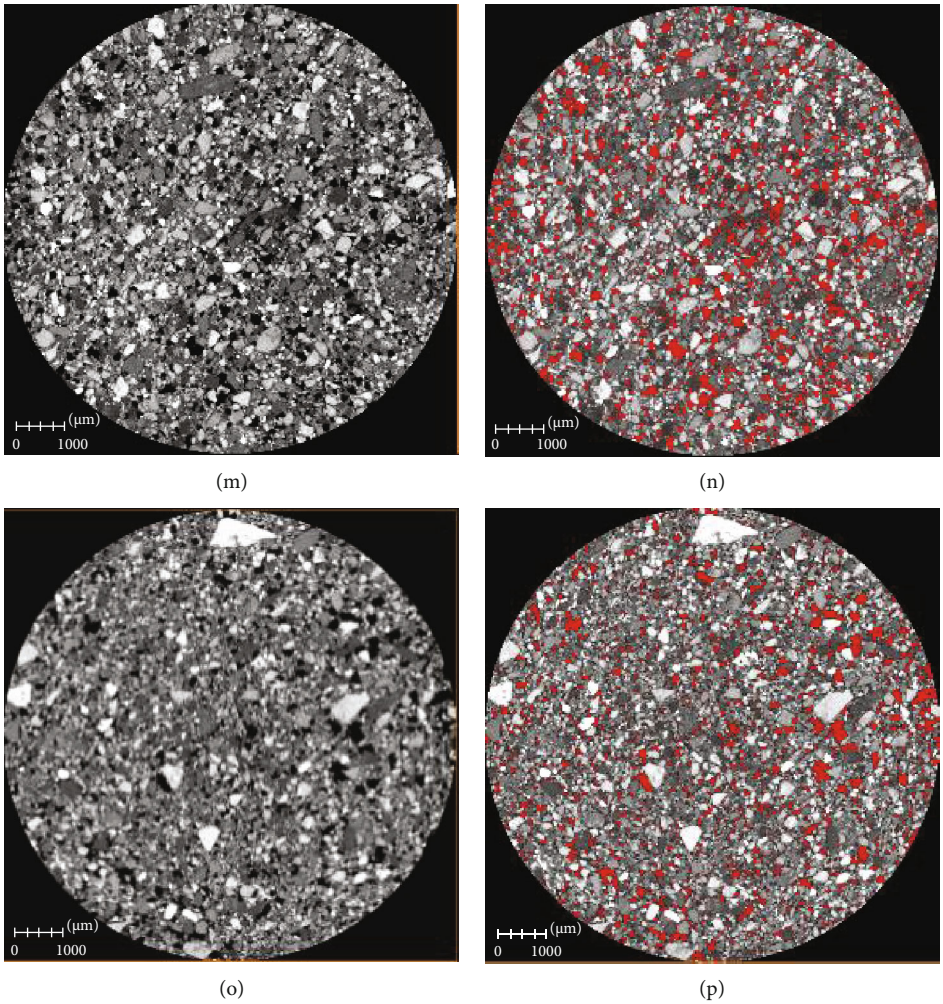

Figure 9: Tailing sand pore threshold segmentation. (a, b) q-1; (c, d) h-1; (e, f) q-2; (g, h) h-2; (i, j) q-3; (k, l) h-3; (m, n) q-4; (o, p) h-4.

4. Experimental Results

4.1. Flow Velocity and Hydraulic Gradient. In the process of the seepage failure experiment, record the seepage flow and sample seepage height (the difference between piezometer tube 1 and tube 4) of the five groups of tailing sand samples at different water head heights. Then, the seepage velocity and hydraulic gradient are calculated. The relationship curve of the hydraulic gradient with seepage velocity and permeability coefficient is shown in Figure 7.

Fine particle tailing sand continuously flowed out from the top of the first group of tailing sand samples during the seepage failure experiment. With the increase of seepage force, microcracks appeared in the middle of the sample and turbidity appeared on the top. According to the relationship curve between seepage velocity and hydraulic gradient in the records, seepage failure has happened in the sample, when the hydraulic gradient of the sample is 3.15. At the same time, the permeability coefficient suddenly increased from $8.98 \times 10^{-4}\,\mathrm{cm} \cdot \mathrm{s}^{-1}$ to $10.22 \times 10^{-4}\,\mathrm{cm} \cdot \mathrm{s}^{-1}$. Combined with the experimental phenomenon, we found that the failure type of tailing sand includes both piping failure and flow soil failure, which is a transitional failure.

In the second and fourth groups of tailing sand sample, cracks appeared in the middle and lower parts of the later stage of seepage failure, and sand boiling appeared on the top. With the increase of seepage force, the cracks of the samples continued to expand to form faults, causing the samples to move from the fault as a whole floating. It can be found from the relationship curve that the permeability coefficient and flow velocity will increase suddenly. The flow soil seepage failure occurred in both samples.

The third and fifth groups of tailing sand samples showed cracks on the top during the seepage process, and fine particle tailing sand continuously flowed out from the top of the samples. With further increase of the water head, the sample cracks expanded rapidly and the seepage flow increased significantly. Finally, the seepage was very cloudy. It can be seen from the relationship curve between flow velocity and hydraulic gradient that the hydraulic slope increases slightly but the velocity increases significantly. The relationship curve between hydraulic gradient and seepage coefficient also shows the same trend. It indicates that piping failure occurred in the samples.

As can be seen from Figure 7, when the samples reach the critical failure, the curve begins to increase sharply, and

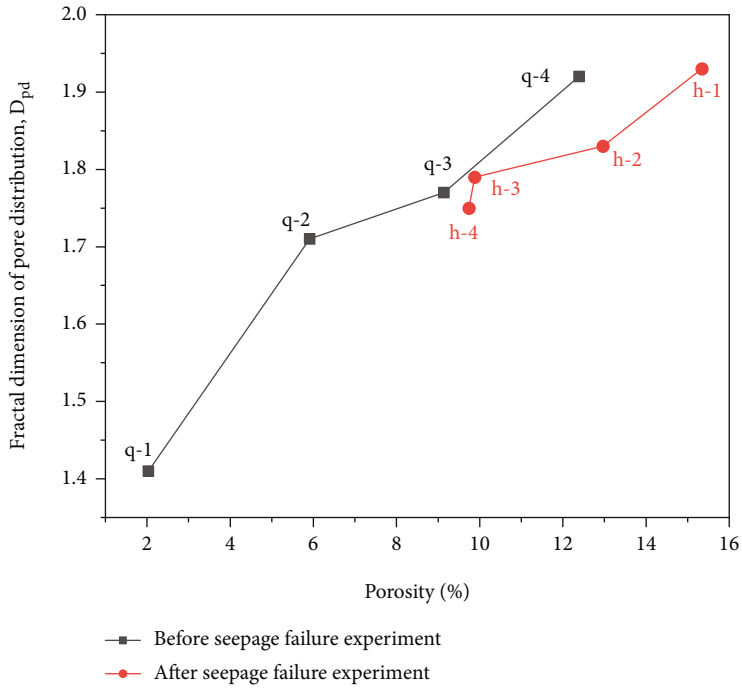

Figure 10: Relationship between porosity and D_{pd} of tailing sand.

the hydraulic gradient at this turning point is the i_{cr}. The i_{cr} of tailing sand of one to five groups are 3.15, 4.95, 4.56, 3.6, and 3.48.

4.2. D_{pd} Feature Analysis of Tailing Sand. The original tailing sand data obtained by X-ray micro-CT scan will be affected by various types of system noise and artifacts [36–38]. Micro-CT system eliminates the image system noise through its local mean filter. Use the Avizo and VG Studio max software to remove false shadows from the image. This improves the accuracy and reliability of the data. Finally, a two-dimensional slice image of the tailing sand sample is obtained, as shown in Figure 8. The low gray values correspond to pores, and the high gray values correspond to tailing sand.

CT scanning technology is used to establish the true mesostructure of tailing sand and obtain the data of porosity, pore volume, pore equivalent diameter, and its number. The image segmentation is performed according to the commonly used Otsu algorithm, and the void ratio obtained from the experiment is compared to determine the optimal segmentation threshold [39]. This method effectively avoids errors in the quantitative analysis of the mesostructure caused by the improper selection of the threshold. Tailing sand pore threshold segmentation is shown in Figure 9, with red representing the pores.

The two-dimensional slice images of the tailing sand sample after threshold segmentation are binarized, and the pore box dimension of the tailing sand sample is calculated by the Image J software. Three binarized images of typical positions are taken for each sample to calculate the pore box dimension, and the average value of the pore box dimension is taken as the D_{pd} of the sample. The corresponding relationship between D_{pd} and porosity is shown in Figure 10.

It can be seen from Figure 10:

(1) After the seepage failure experiment, the porosity of the first layer and the second layer of the tailing sand sample increased significantly by 13.31% and 7.05%, and the corresponding D_{pd} also increased, respectively, by 0.52 and 0.12. Because the fine tailing sand particles of the first and second layers migrate to the skeleton structure of the third and fourth layers along the seepage direction under the action of seepage force, the porosity increases

(2) The porosity of the third layer tailing sand only increases by 0.74%, and there is little change in the corresponding D_{pd} from 1.77 to 1.79. It is because the fine tailing sand particles in the first and second layers flow into the third layer, and the fine tailing sand particles in their particle skeleton also migrate to the fourth layer along the seepage direction under the action of seepage force. However, the inflow of fine tailing sand particles is less than the migration

(3) The porosity of the fourth layer tailing sample after seepage failure decreases from, and the corresponding D_{pd} decreases from 1.92 to 1.75. It indicates that the fine tailing sand particles from the first layer to the third layer migrate to the fourth layer, and the porosity of the fourth layer tailing sand decreases significantly

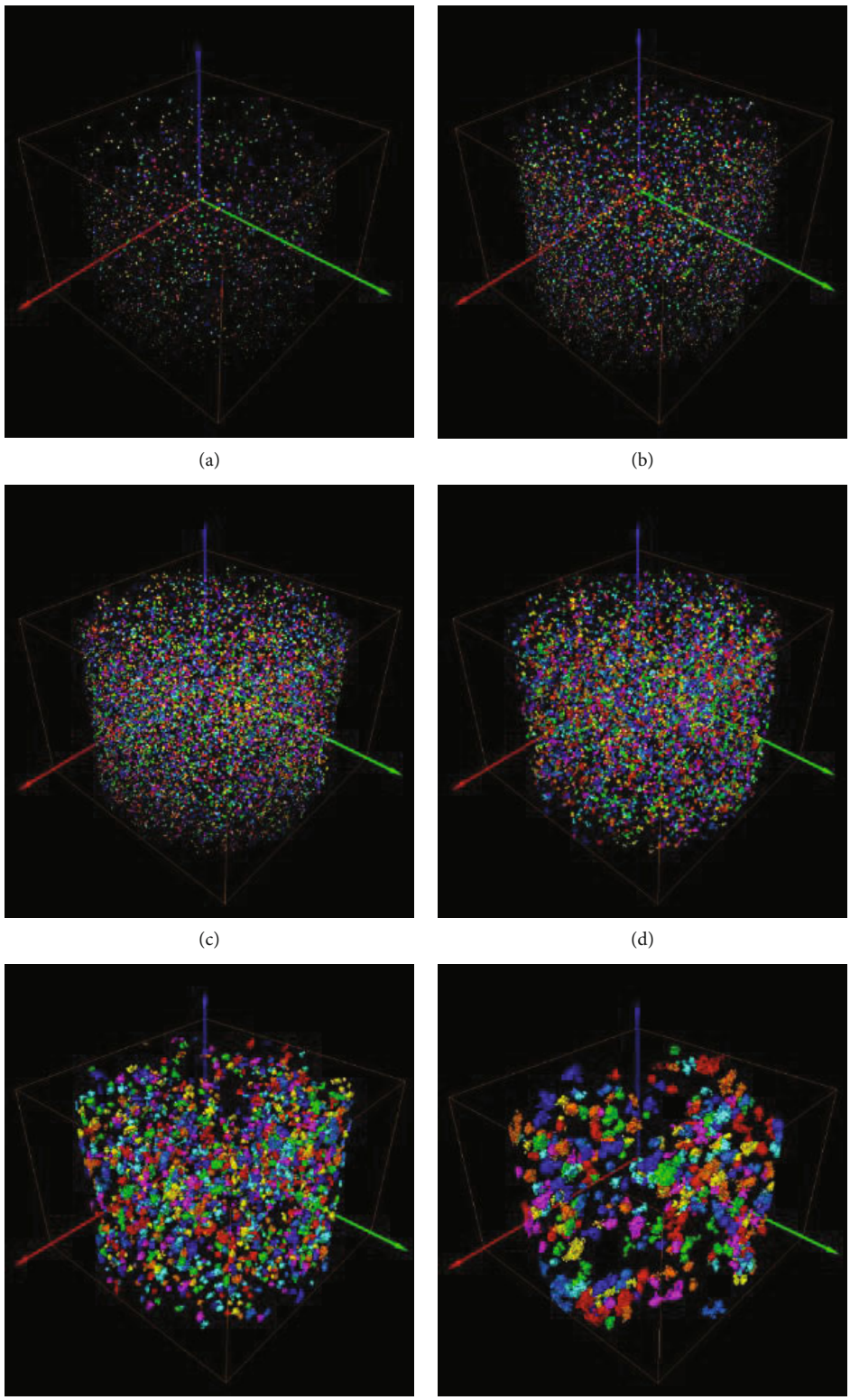

(a) (b) (c) (d) (e) (f)

Figure 11: Continued.

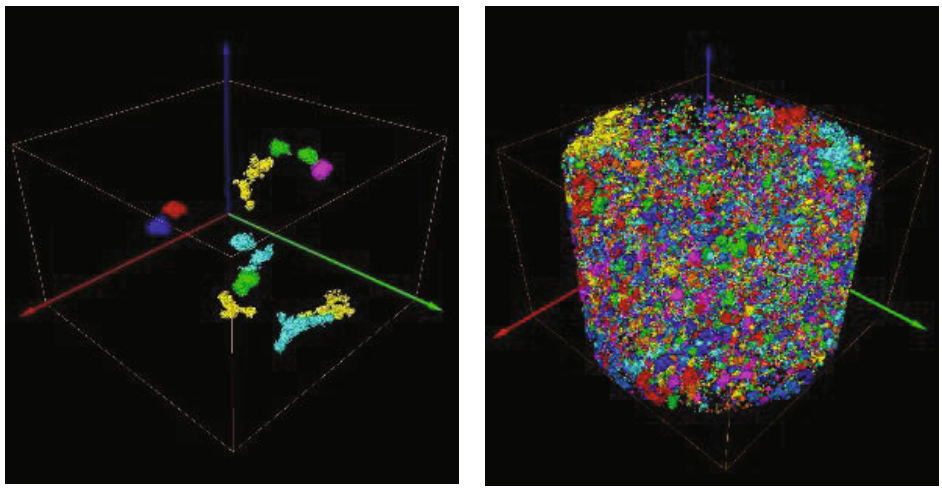

(g) (h)

Figure 11: Three-dimensional graphics of pores with different pore sizes of q-1: (a) 9 μm-18 μm; (b) 18 μm-36 μm; (c) 36 μm-72 μm; (d) 72 μm-144 μm; (e) 144 μm-288 μm; (f) 288 μm-576 μm; (g) >576 μm; (h) >9 μm.

(4) The D_{pd} and porosity show a relatively obvious positive correlation. When the porosity increases, the D_{pd} increases, indicating that the larger the pore distribution area is, the more loose the tailing particles are; when the porosity decreases, the D_{pd} decreases correspondingly, indicating that the smaller pore distribution area is, the closer the tailing sand particles are. The D_{pd} of tailing sand characterizes the changed feature of pore distribution

4.3. D_{ps} Feature Analysis of Tailing Sand. The pore size distribution of tailing sample is obtained through the label analysis and analysis filter analysis modules in the Avizo 3D visualization software. Surface view module is used to display the pores after threshold segmentation. Topological triangular connection is carried out by generating tetra grid, and then, label analysis is used to identify the boundaries of single pores and mark them to generate pore space marking images. Finally, the pore size is classified and extracted by the analysis filter module. Figure 11 shows the distribution of pores with different pore sizes in layer q-1.

According to the different pore sizes and their numbers of all tailing sand samples, using formula (2) to calculate D_{ps}, the relationship between D_{ps} and porosity before and after the tailing sand seepage failure is shown in Figure 12. The results show the following: before the tailing sand seepage failure, the porosity of the first to fourth layers increases from 2.03% to 12.4%, and the corresponding D_{ps} increases from 1.25 to 1.58. After the tailing sand seepage failure, the porosity of the first and second layers increases to 15.34% and 12.96%, and the corresponding D_{ps} increases to 1.81 and 1.60. The porosity of the third layer only increased by 0.74%, and the corresponding D_{ps} did not change much. The porosity of the fourth layer decreases clearly, and so does the D_{ps}. Interestingly, before the seepage failure experiment, the porosity of the fourth layer did not increase sharply, but the D_{ps} increases sharply. It shows that the uniformity of pore size of tailing sand in the fourth layer decreases, and the size difference between pores is great. D_{ps} shows a positive correlation with porosity before and after tailing sand seepage failure, and D_{ps} is closely related to the uniformity of pore size. D_{ps} reflects the variation characteristics of pore number distribution with different pore sizes.

4.4. D_m Feature Analysis of Tailing Sand Seepage. The relationship between the D_m of tailing sand of each group and the particle size structure of tailing sand, average permeability coefficient, and i_{cr} is shown in Table 3.

Comparing the D_m and particle size structure of tailing sand, we find that

(1) With the increase of the D_m of tailing samples, the C_u reflecting the characteristics of particle size tends to increase, because the D_m characterizes the gradual accumulation of tailing sand particles. The larger D_m is, the more particles are accumulated step by step in a certain volume of soil, the slower the particle separation curve is, the higher particle nonuniformity is, and the larger the C_u value is

(2) The first group and the second group of tailing sand are relatively similar in fine particle content, and the particle size curve is different while maintaining the same dry density. When the D_m of the tailing sand sample is larger, the limiting particle size d_{60} of the sample tends to increase, k increases, and the i_{cr} for seepage failure decreases. Because with the increase of the D_m, the content of particles smaller than a certain particle size decreases, the average permeability coefficient increases, and the i_{cr} decreases. The comparison between the third group and the fourth group of tailing sand sample also shows that when

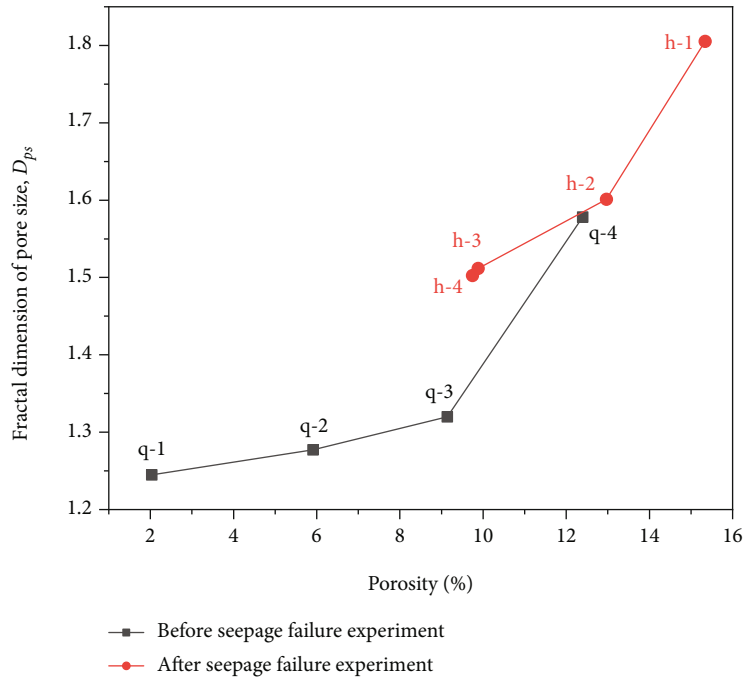

Figure 12: Relationship between D_{ps} and porosity of tailing sand.

Table 3: Comparison table of D_m and particle size structure of tailing sand.

Groups	d_{60} (μm)	C_u	C_c	i_{cr}	Average permeability coefficient, $\bar{k}$ (10^{-4} cm·s^{-1})	D_m
First	147.96	3.14	1.01	3.15	8.09	1.7498
Second	137.96	2.92	0.63	4.95	3.35	1.6472
Third	106.85	3.50	1.23	4.56	2.27	1.8256
Fourth	61.58	3.06	1.15	3.6	1.62	1.7007
Fifth	136.03	3.42	1.15	3.48	4.56	1.7805

the D_m increases, the d_{60} and C_u of tailing sand samples tend to increase

(3) In fact, the D_m of tailing sand mainly reflects the change rule parameter of the cumulative content of particles smaller than a certain size. When the D_m is large, it means that the cumulative content of particles smaller than a certain size decreases. Particle distribution curve will be relatively flat, and the C_u of tailing sand tends to increase. Therefore, the D_m can be regarded as a parameter to characterize the structure of tailing sand. D_m reflects the relationship between the internal structural characteristics of tailing sand and parameters such as particle distribution curve, permeability, and C_u. D_m affects the seepage failure characteristics of tailing sand

The relationship between D_m and i_{cr} of the tailing sand sample is shown in Figure 13. The D_m of tailing sand has a significant quadratic function relationship with the i_{cr}. On the left side of the image, with the increase of the D_m, the nonuniformity of the tailing sand sample increases, and the nonuniformity of the particle distribution will affect the permeability, leading to the i_{cr} decrease. On the right side of the image, with the increase of the D_m, the C_u of tailing sand further increases. However, the bite force between the tailing sand particles gradually increased, the permeability of the tailing sand samples weakened, the permeability coefficient decreased, and the i_{cr} increased accordingly.

5. Discussions

The seepage failure of fine-grained tailing sand is due to the migration of fine particles, which changes the pore characteristics and reduces the structure of the tailing sand. D_{pd} and D_{ps} provide suitable mathematical tools for analyzing the changes in the pore structure of tailing sand during seepage failure [40]. D_{pd} and D_{ps} can reflect the influence law of particle migration on the pore structure during the seepage failure of tailing sand. The D_{pd} can quantitatively characterize the pore distribution characteristics of tailing sand. The D_{ps} can quantitatively characterize the pore number distribution characteristics of tailing sand with different pore sizes. D_{pd} and D_{ps} gradually decrease along the seepage direction, because the fine particles of tailing sand migrate along the seepage direction during seepage failure. Thus,

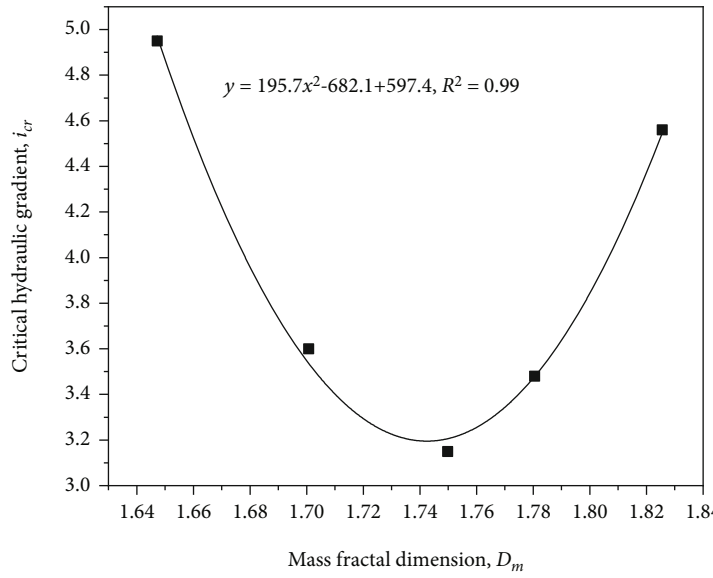

Figure 13: Relationship curve between D_m and i_{cr}.

Table 4: Comparison of seepage failure type with different judgment methods.

Groups	Experimental results	C_u method	Pore diameter and fine particle diameter comparison method	Fine particle content method	D_m method
First	Transitional	Flow soil	Piping	Piping	Flow soil
Second	Flow soil	Flow soil	Flow soil	Flow soil	Flow soil
Third	Piping	Flow soil	Flow soil	Piping	Piping
Fourth	Flow soil	Flow soil	Flow soil	Flow soil	Flow soil
Fifth	Piping	Flow soil	Flow soil	Transitional	Piping

the porosity gradually decreases, and the heterogeneity of pore size gradually decreases. D_{pd} and D_{ps} provide new ideas to prevent tailing sand seepage failure. Some studies show that adding flocculants to the tailing slurry changes the structure of settling particles and improves the permeability of tailing sand. It also increases D_{pd} and D_{ps} correspondingly, thus improving the safety and stability of the tailing dam [41, 42].

According to Figure 13, the general functional expression of tailing sand i_{cr} and D_m is as follows:

$$i_{cr} = A(D_m - D_{m0})^2 + B, \tag{11}$$

where D_{m0} is the critical mass fractal dimension for the variation of seepage failure type of tailing sand; A and B are the structural parameters of the tailing sand, which are related to the particle size and gradation of the tailing sand.

When $D_m < D_{m0}$, the nonuniformity of tailing sand increases with the increase of D_m at the same dry density. However, the C_u is small, which weakens the bite force between the particles, and the i_{cr} is reduced. At the same time, due to the high density of the tailing sand, the small porosity, and pore diameter, the fine tailing sand particles cannot quickly pass through the pores formed by the coarse particles, so it is easy to occur flow soil failure.

When $D_m > D_{m0}$, the nonuniformity of tailing sand further increases with the increase of D_m at the same dry density. The bite force between the particles gradually increased, and the i_{cr} gradually increased. However, the pore sizes formed between the coarse particles also increase, the fine particles pass through the pores of coarse particles more easily, and the tailing sand is prone to piping failure.

The D_m judgment method is compared with the experimental phenomenon and the traditional seepage failure type judgment method, such as the C_u method, pore diameter and fine particle diameter comparison method, and fine particle content method. The results are shown in Table 4.

Comparing different discriminant methods, it is found that the discriminant results of several discriminant methods are basically consistent with the experimental results. Among them, the discriminant method of fine particle content method and D_m method is the most accurate, which verifies the reliability of the D_m method in judging the type of seepage failure. However, there are differences between the two discriminant methods for the first group of samples, which is consistent with the fact that this group of samples is in transitional failure. In practical applications, the D_m method can be mutually verified with the fine particle content method, which can improve the accuracy of the identification of the tailing sand seepage failure type.

6. Conclusions

This paper studies the fractal characteristics of the mesostructure before and after the tailing sand seepage failure and proposes the D_m method to distinguish the seepage failure type of tailing sand. The main conclusions are summarized as follows:

(1) Before and after the seepage failure experiment, the D_{pd} and porosity show a relatively obvious positive correlation. The fine tailing sand particles migrate and flow along the seepage direction under the action of seepage force, which changes the skeleton of the tailing sand particles. When the porosity of tailing sand increases, the D_{pd} increases accordingly. The larger the distribution area of the pores, the looser the tailing sand particles. When the porosity decreases, the D_{pd} decreases correspondingly, which means that the smaller the distribution area of the pores, the closer the tailing sand particles. The D_{pd} of tailing sand characterizes the changed feature of pore distribution

(2) Before and after tailing sand seepage failure, the D_{ps} and porosity show a positive correlation. When the porosity increases, the D_{ps} increases. When the porosity decreases, the D_{ps} decreases correspondingly. The D_{ps} reflects the variation characteristics of pore number distribution with different pore sizes

(3) The D_m of tailing sand mainly reflects the change rule parameter of the cumulative content of particles smaller than a certain size. Therefore, the D_m can be regarded as a parameter to characterize the structure of tailing sand, which reflects the relationship between the internal structural characteristics of tailing sand and parameters such as particle distribution curve, C_u, and average permeability coefficient

(4) The D_m of tailing sand and the i_{cr} present a significant quadratic function relationship. According to the relationship between the D_m and the critical mass fractal dimension (D_{m0}), the seepage failure type of fine-grained tailing sand can be distinguished. When $D_m < D_{m0}$, the tailing sand is prone to flow soil type seepage failure, while when $D_m > D_{m0}$, the tailing sand is prone to piping type seepage failure. The D_m discrimination method is compared with the experimental phenomenon and the traditional discrimination method of seepage failure type, which verifies the accuracy of D_m discrimination of tailing sand seepage failure type. The D_m method has a certain reference significance for the treatment of the seepage failure of the tailing dam

Data Availability

The experimental data used to support the findings of this study are included within the article.

Conflicts of Interest

The authors declare no conflict of interest.

Acknowledgments

This research was supported by the National Key Research and Development Plan of China (No. 2017YFC0804609).

References

[1] G. Z. Yin, Q. G. Zhang, W. S. Wang, Y. L. Chen, W. L. Geng, and H. R. Liu, "Experimental study on the mechanism effect of seepage on microstructure of tailings," *Safety Science*, vol. 50, no. 4, pp. 792–796, 2012.

[2] R. Chen, W. D. Lei, and Z. H. Li, "Anisotropic shear strength characteristics of a tailings sand," *Environmental Earth Sciences*, vol. 71, no. 12, pp. 5165–5172, 2014.

[3] Y. H. Yang, Z. A. Wei, A. Fourie et al., "Particle shape analysis of tailings using digital image processing," *Environmental Science and Pollution Research*, vol. 26, no. 25, pp. 26397–26403, 2019.

[4] M. T. Zandarin, L. A. Decop, R. Rodriguez, and F. Zabala, "The role of capillary water in the stability of tailing dams," *Engineering Geology*, vol. 105, no. 1-2, pp. 108–118, 2009.

[5] Q. G. Zhang, G. Z. Yin, Z. A. Wei, X. Y. Fan, W. S. Wang, and W. Nie, "An experimental study of the mechanical features of layered structures in dam tailings from macroscopic and microscopic points of view," *Engineering Geology*, vol. 195, pp. 142–154, 2015.

[6] C. Zhang, H. M. Liu, C. H. Yang, and S. W. Wu, "Mechanical characteristics of non-saturated tailings and dam stability," *International Journal of Mining Reclamation and Environment*, vol. 31, no. 8, pp. 530–543, 2017.

[7] G. S. Cao, W. S. Wang, G. Z. Yin, and Z. A. Wei, "Experimental study of shear wave velocity in unsaturated tailings soil with variant grain size distribution," *Construction and Building Materials*, vol. 228, article 116744, 2019.

[8] Q. L. Chen, C. Zhang, C. H. Yang, C. K. Ma, Z. K. Pan, and J. J. K. Daemen, "Strength and deformation of tailings with fine-grained interlayers," *Engineering Geology*, vol. 256, pp. 110–120, 2019.

[9] Q. Bi, C. H. Li, and J. X. Chen, "Effect of fine particle content on mechanical properties of tailings under high confining pressure," *Arabian Journal of Geosciences*, vol. 14, no. 11, pp. 942–954, 2021.

[10] L. Clarkson and D. Williams, "An overview of conventional tailings dam geotechnical failure mechanisms," *Mining Metallurgy & Exploration*, vol. 38, no. 3, pp. 1305–1328, 2021.

[11] C. H. Yang, C. Zhang, Q. M. Li, Y. Z. Yu, C. K. Ma, and Z. J. Duan, "Disaster mechanism and prevention methods of large-scale high tailings dam," *Rock Soil mechanics*, vol. 2021, no. 1, pp. 1–17, 2021.

[12] Y. Q. Shi, C. H. Li, and D. Y. Long, "Study of the microstructure characteristics of three different fine-grained tailings sand samples during penetration," *Materials*, vol. 13, no. 7, p. 1585, 2020.

[13] B. B. Mandelbort, *The Fractal Geometry of Nature*, W.H. Freeman and Company, New York, NY, 1982.

[14] D. L. Turcotte, "Fractals and fragmentation," *Journal of Geophysical Research: Earth Surface*, vol. 91, no. B2, pp. 1921–1926, 1986.

[15] S. W. Tyler and S. W. Wheatcraft, "Fractal scaling of soil particle-size distributions: analysis and limitations," *Soil Science Society of America Journal*, vol. 56, no. 2, pp. 362–369, 1992.

[16] Z. Song, Y. Wang, H. Konietzky, and X. Cai, "Mechanical behavior of marble exposed to freeze-thaw-fatigue loading," *International Journal of Rock Mechanics and Mining Sciences*, vol. 138, article 104648, 2021.

[17] Y. Wang, B. Zhang, B. Li, and C. H. Li, "A strain-based fatigue damage model for naturally fractured marble subjected to freeze-thaw and uniaxial cyclic loads," *International Journal of Damage Mechanics*, vol. 30, no. 10, pp. 1594–1616, 2021.

[18] C. M. Mahdi and M. R. D. Ghaleno, "Evaluating fractal dimension of the soil particle size distributions and soil water retention curve obtained from soil texture components," *Archives of Agronomy and Soil Science*, vol. 66, no. 12, pp. 1668–1678, 2020.

[19] K. Peng, Z. P. Liu, Q. L. Zou, Q. H. Wu, and J. Q. Zhou, "Mechanical property of granite from different buried depths under uniaxial compression and dynamic impact: an energy-based investigation," *Powder Technology*, vol. 362, pp. 729–744, 2020.

[20] X. Y. Zou, Z. D. Zhang, M. Y. Wu, and Y. Q. Wan, "Slope-scale spatial variability of fractal dimension of soil particle size distribution at multiple depths," *Soil Science Society of America Journal*, vol. 85, no. 1, pp. 117–131, 2021.

[21] C. Atzeni, G. Pia, U. Sanna, and N. Spanu, "A fractal model of the porous microstructure of earth-based materials," *Construction and Building Materials*, vol. 22, no. 8, pp. 1607–1613, 2008.

[22] G. L. Tao and J. R. Zhang, "Two categories of fractal models of rock and soil expressing volume and size-distribution of pores and grains," *Chinese Science Bulletin*, vol. 54, no. 23, pp. 4458–4467, 2009.

[23] A. J. Katz and A. H. Thompson, "Fractal sandstone pores: implications for conductivity and pore formation," *Physical Review Letters*, vol. 54, no. 12, pp. 1325–1328, 1985.

[24] M. V. S. Bonala and L. N. Reddi, "Fractal representation of soil cohesion," *Journal of Geotechnical and Geoenvironmental Engineering*, vol. 125, no. 10, pp. 901–904, 1999.

[25] Y. F. Xu, "Fractal approach to unsaturated shear strength," *Journal of Geotechnical and Geoenvironmental Engineering*, vol. 130, no. 3, pp. 264–273, 2004.

[26] B. M. Yu, "Analysis of flow in fractal porous media," *Applied Mechanics Reviews*, vol. 61, no. 5, article 050801, 2008.

[27] P. Xu, "A discussion on fractal models for transport physics of porous media," *Fractals*, vol. 23, no. 3, article 1530001, 2015.

[28] J. C. Cai, W. Wei, X. Y. Hu, and D. A. Wood, "Electrical conductivity models in saturated porous media: a review," *Earth-Science Reviews*, vol. 171, pp. 419–433, 2017.

[29] Y. Wang, W. K. Feng, R. L. Hu, and C. H. Li, "Fracture evolution and energy characteristics during marble failure under triaxial fatigue cyclic and confining pressure unloading (FC-CPU) conditions," *Rock Mechanics and Rock Engineering*, vol. 54, no. 2, pp. 799–818, 2021.

[30] W. D. Jiang, "Fractal character of lenticles and its influence on sediment state in tailings dam," *Journal of Central South University of Technology*, vol. 12, no. 6, pp. 753–756, 2005.

[31] Q. G. Zhang, G. Z. Yin, X. Y. Fan, Z. A. Wei, W. S. Wang, and W. Nie, "Loading capacity and deformation characteristics of tailings based on a fractal geometrical analysis of the particle microstructure," *Minerals*, vol. 5, no. 1, pp. 86–103, 2015.

[32] E. Perfect and B. D. Kay, "Applications of fractals in soil and tillage research: a review," *Soil and Tillage Research*, vol. 36, no. 1-2, pp. 1–20, 1995.

[33] S. Ersahin, H. Gunal, T. Kutlu, B. Yetgin, and S. Coban, "Estimating specific surface area and cation exchange capacity in soils using fractal dimension of particle-size distribution," *Geoderma*, vol. 136, no. 3-4, pp. 588–597, 2006.

[34] R. R. Filgueira, L. L. Fournier, C. I. Cerisola, P. Gelati, and M. G. Garcia, "Particle-size distribution in soils: a critical study of the fractal model validation," *Geoderma*, vol. 134, no. 3-4, pp. 327–334, 2006.

[35] N. Prosperini and D. Perugini, "Particle size distributions of some soils from the Umbria Region (Italy): fractal analysis and numerical modelling," *Geoderma*, vol. 145, no. 3-4, pp. 185–195, 2008.

[36] Y. Wang, J. Q. Han, Z. Y. Song, and C. Zhu, "Macro-meso failure behavior of pre-flawed hollow-cylinder granite under multi-level cyclic loads: insights from acoustic emission and post-test CT scanning," *Engineering Fracture Mechanics*, vol. 258, article 108074, 2021.

[37] N. Saxena, R. Hofmann, F. O. Alpak, J. Dietderich, S. Hunter, and R. J. Day-Stirrat, "Effect of image segmentation & voxel size on micro-CT computed effective transport & elastic properties," *Marine and Petroleum Geology*, vol. 86, pp. 972–990, 2017.

[38] J. P. Mathews, Q. P. Campbell, H. Xu, and P. Halleck, "A review of the application of X-ray computed tomography to the study of coal," *Fuel*, vol. 209, pp. 10–24, 2017.

[39] N. Otsu, "A threshold selection method from gray-level histogram," *IEEE Transactions on Systems, Man, and Cybernetics*, vol. 9, no. 1, pp. 62–66, 1979.

[40] R. Uthayakumar, G. A. Prabakar, and S. A. Azis, "Fractal analysis of soil pore variability with two dimensional binary images," *Fractals*, vol. 19, no. 4, pp. 401–406, 2011.

[41] C. H. Li, Y. Q. Shi, P. Liu, and N. Guo, "Analysis of the sedimentation characteristics of ultrafine tailings based on an orthogonal experiment," *Advances in Materials Science and Engineering*, vol. 2019, Article ID 5137092, 2019.

[42] D. Zheng, W. D. Song, Y. Y. Tan, S. Cao, Z. L. Yang, and L. J. Sun, "Fractal and microscopic quantitative characterization of unclassified tailings flocs," *International Journal of Minerals Metallurgy and Materials*, vol. 28, no. 9, pp. 1429–1439, 2021.